Colloid Polym Sci (2009) 287:819–827
DOI 10.1007/s00396-009-2036-x

ORIGINAL CONTRIBUTION

Effects of concentration of nonionic surfactant and molecular weight of polymers on the morphology of anisotropic polystyrene/poly(methyl methacrylate) composite particles prepared by solvent evaporation method

Xueping Ge · Mozhen Wang · Xiang Ji · Xuewu Ge · Huarong Liu

Received: 27 October 2008 / Revised: 23 February 2009 / Accepted: 2 April 2009 / Published online: 5 May 2009

Abstract The effects of the concentration of polyoxyethylene octylphenyl ether (OP-10) as a nonionic surfactant and the molecular weight of polymers (polystyrene (PS) and poly(methyl methacrylate) (PMMA)) on the morphology of anisotropic PS/PMMA composite particles were investigated. In the case of polymers with lower molecular weight ($M_w \approx 6.0 \times 10^4$ g/mol), the PS/PMMA composite particles have dimple, via acorn, to hemispherical shapes along with the increase of the OP-10 concentration. On the other hand, when the polymers have higher molecular weight ($M_w \approx 3.3 \times 10^5$ g/mol), the morphology of PS/PMMA composite particles changed from dimple, via hemispherical, to snowman-like structure while the concentration of OP-10 was increased. Furthermore, thermodynamic analysis was first simply made by spreading coefficients, and the results indicated that both the concentration of OP-10 aqueous solution and the molecular weight of polymers were very important to the final morphology of anisotropic composite particles.

Keywords Anisotropic PS/PMMA composite particles · Concentration of OP-10 · Interfacial tension · Molecular weight · Nonionic surfactant · Spreading coefficients

X. Ge · M. Wang (✉) · X. Ji · X. Ge (✉) · H. Liu
CAS Key Laboratory of Soft Matter Chemistry,
Department of Polymer Science and Engineering,
University of Science and Technology of China,
Hefei, Anhui 230026, China
e-mail: pstwmz@ustc.edu.cn
e-mail: xwge@ustc.edu.cn

Introduction

In recent years, great interest has been focused on anisotropic particles, which is anisotropic in shape and/or surface chemistry. Because of their unique properties, anisotropic particles could be very useful for controlling light scattering [1], fluid properties [2, 3], molecular recognition [4–6], self-assembling process [7, 8], and forming pickering emulsions [9–11].

Synthesis of anisotropic particles is one of the very intriguing and challenging aspects in current materials science. A few of successful methods have been developed [8, 12–35]. For example, solvent evaporation method is a practical way to fabricate anisotropic composite particles [36–39]. Okubo et al. prepared polystyrene (PS)/poly(methyl methacrylate) (PMMA) composite particles by release of solvent from droplets containing dissolved PS and PMMA, which were dispersed in surfactant aqueous solution. When poly(vinyl alcohol) (PVA) was used as a surfactant, nonspherical PS/PMMA composite particles with a single dimple were obtained [36]. When sodium dodecyl sulfate (SDS) was used in place of PVA, the shape of the composite particles would change from the dimple, via acorn, to spherical with the increase of SDS concentration [37]. Recently, Okubo et al. prepared composite PS/PMMA particles employing polyoxyethylene nonylphenyl ether (Emulgen 911) as a nonionic surfactant [39, 40]. The effect of partitioning of Emulgen 911 between oil and water on the phase separation of PS and PMMA so as to form anisotropic composite particles was first examined, but it is still not sufficiently. For example, the molecular weight of polymer is believed to play an important role on the morphology of final particles [19, 41–43], which could

affect the interfacial tension. However, the study of effect of molecular weight of polymer on the final morphology of anisotropic composite particles prepared by solvent evaporation method was limited [40]. Furthermore, thermodynamic analysis about total interfacial free energy change in the previous reports was very complex [36–40]. Therefore, a simple way to analyzing the influence factors to final morphology of composite particles is critical needed.

In this paper, a nonionic surfactant, polyoxyethylene octylphenyl ether (OP-10), was used to prepare the PS/PMMA anisotropic composite particles by release of toluene from the polymer/ toluene (1/12, *w*/*w*) droplets which were dispersed in various concentration of OP-10 aqueous solutions. The influence of concentration of OP-10 and molecular weight of PS and PMMA on the final morphology of anisotropic PS/PMMA composite particles had been studied in detail. In order to simplify the thermodynamic analysis, spreading coefficients were first used to analyzing the influence factors to final morphology of composite particles.

Experimental

Materials

Styrene (S) and methyl methacrylate (MMA) were purified by passing through a basic alumina column to remove the inhibitor before use. Reagent grade 2,2′-azobis(isobutyronitrile) (AIBN) was purified by recrystallization in methanol. Polyoxyethylene octylphenyl ether (with ten EO units; Reagent Grade), toluene (Analytical Reagent), and methanol (Analytical Reagent) were used as received from Shanghai Chemical Reagents Co., China.

Preparation of PS/PMMA composite particles

PS and PMMA were prepared under the conditions listed in Table 1. The homopolymers were precipitated by pouring polymer solution into tenfold excess methanol and collected by filtration, then dried in vacuum oven at room temperature. The prepared PS and PMMA were dissolved in toluene (PS/PMMA/toluene=1/1/24, *w*/*w*/*w*), then the resulting solution (1.3 g) was mixed with various concentrations (6.3×10^{-4}, 0.01, 0.34, and 0.67 wt.% relative to water) of OP-10 aqueous solutions (30 g). The resultant mixtures were stirred vigorously in a 150-ml beaker. Subsequently, toluene was evaporated from the dispersions by stirring with a magnetic stirrer at room temperature for 24 h (surface area between dispersion and air was 30 cm^2). The particles were collected by centrifugation. After washed with ethanol three times, the PS/PMMA composite particles were dispersed in ethanol for storage.

Characterization of molecular weight of polymer

The weight average molecular weights (M_w) and polydispersities (M_w/M_n) of the prepared PS and PMMA were measured by gel permeation chromatography on a Waters 150C instrument equipped with 10^3, 10^4, and 10^5 Å Waters Ultrastyragel columns and using tetrahydrofuran as an eluent at a rate of 1.0 ml/min. Calibration was against polystyrene standards.

Observation of the composite polymer particles

The PS/PMMA composite polymer particles were observed by field-emission scanning electron microscopy (FESEM; JEOL JSM-6700, the acceleration voltage of FESEM is 5 kV) and transmission electronic microscopy (TEM; Hitachi H-800, 200 kV). Samples for TEM and SEM analysis were prepared at room temperature by dispersing one drop of ethanol solution of the sample on copper grid and then drying in air.

Partition of nonionic surfactant between toluene and water

The partition isotherm of OP-10 between toluene and water was obtained as follows: Toluene (0.6, 0.5, 0.4, 0.3, 0.2, 0.1 g) and OP-10 aqueous solutions at various concentration (6.3×10^{-4}, 0.01, 0.34, and 0.67 wt.% relative to water; 15 g) were mixed in the beakers firstly. After stirred with a magnetic stirrer for 1 h and ultrasonicated for 30 min, the emulsion was put aside at room temperature for 24 h.

Table 1 Preparation of polystyrene and poly(methyl methacrylate)

	Styrene (g)	Methyl methacrylate (g)	Toluene (g)	AIBN (mg)	M_w ($\times10^4$ g/mol)	M_w/M_n
L-PS[a]	20.0		13.0	59	6.1	1.9
H-PS[a]	10.0			10	33.6	2.0
L-PMMA[b]		14.0	21.0	440	6.8	1.5
H-PMMA[a]		6.5	5.0	100	33.1	1.7

[a] Polymerization was conducted at 60°C and bubbled with N_2 for 24 h

[b] Polymerization was conducted at 70°C and bubbled with N_2 for 24 h

Subsequently, the emulsion was separated into the aqueous and toluene phases by centrifugation. The OP-10 concentration in the aqueous phase was measured with a UV2401 PC spectrophotometer (Sahimadzu Corporation, Japan), while that in the toluene phase was calculated by mass balance. In addition, the partition of toluene to the aqueous phase will influence the UV analysis due to the absorbance of toluene at the same wavelength. So, in our experiment, the aqueous phase was stirred for 2 days at room temperature before characterizing by UV in order to evaporate the toluene and a certain amount of water was added to compensate the water losing.

Interfacial tension measured by the ring method

Interfacial tension between the polymer–toluene solution and the aqueous solutions ($\gamma_{P-T/W}$) was measured by the ring method with KRUSS digital tensiometer K9 at room temperature (25°C). The sample vessel was added with the OP-10 aqueous solution firstly, and then it was placed on the sample support. The sample stage was raised until the ring was immersed in the liquid. Polymer solution of toluene was then added slowly. Finally, the sample stage was lowered slowly until the displayed data exceeded the maximum value.

Interfacial tension between PS–toluene phase and PMMA–toluene phase ($\gamma_{PS-T/PMMA-T}$) were measured as follows: PS and PMMA were dissolved in a certain amount of toluene. Then, the resulting solution was left standing for 3 days. Finally, it was separated into PS and PMMA phases clearly, and the layers were separated. The sample vessel was first added with PMMA phase separated from the lower layer, and the sample stage was raised until the ring was immersed in the PMMA phase. Then, PS phase was added slowly. The vessel was sealed and left standing for 1 h until the two phases were stable. Finally, the sample stage was lowered slowly until the displayed data exceeded the maximum value.

Results and discussions

Morphology observation

Figures 1 and 2 showed the SEM and TEM images of anisotropic PS/PMMA (1/1, *w*/*w*) composite particles prepared by release of toluene for 24 h from PS/PMMA/toluene (1/1/24, *w*/*w*/*w*) droplets dispersed in aqueous solution at various OP-10 concentrations (6.3×10^{-4}, 0.01, 0.34, and 0.67 wt.% relative to water). The molecular weight of prepared PS and PMMA was listed in Table 1. The polymers in Figs. 1 A1–A4 and 2 A1–A4 have a relative lower molecular weight, which were identified as L-PS and L-PMMA, while the polymers in Figs. 1 B1–B4

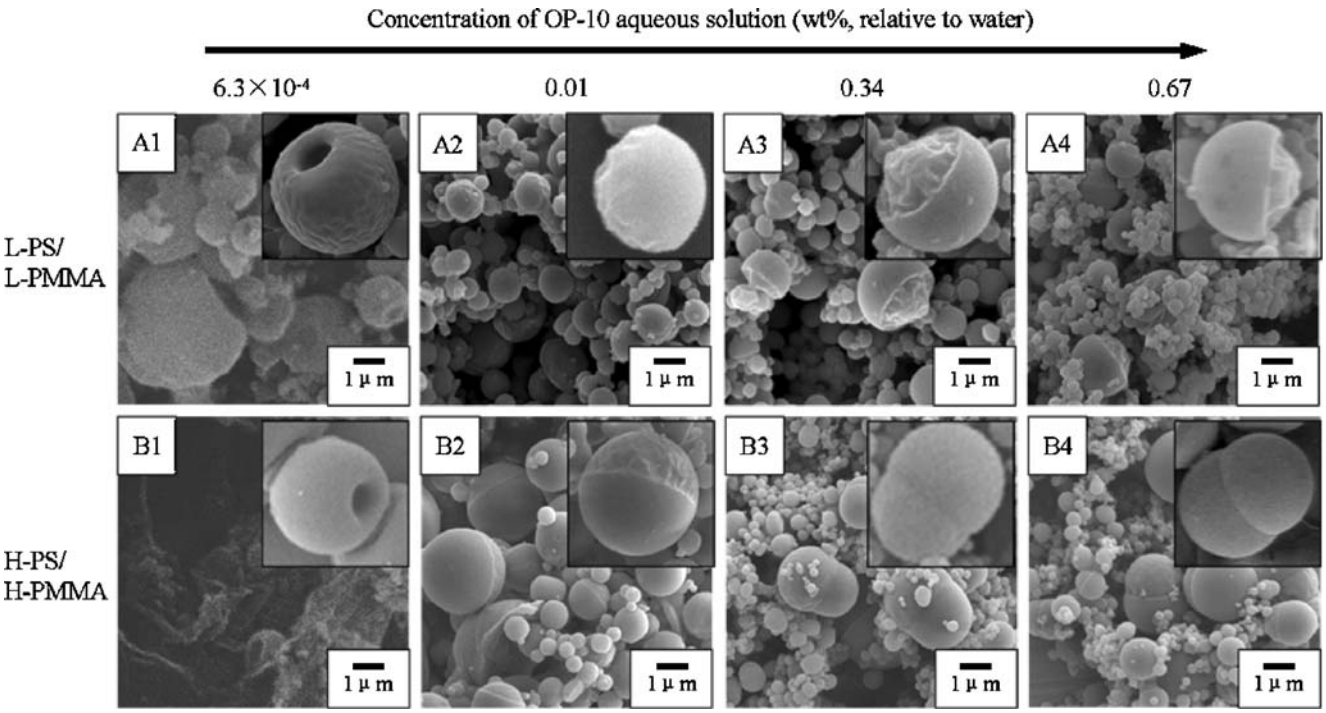

Fig. 1 SEM photographs of PS/PMMA (1/1, *w*/*w*) composite particles prepared by release of toluene from polymer/toluene=1/12 droplets dispersed in various concentration of OP-10 aqueous solutions (weight percent, relative to water): *A1*, *B1* 6.3×10^{-4}; *A2*, *B2* 0.01; *A3*, *B3* 0.34; *A4*, *B4* 0.67. *A1–A4* L-PS and L-PMMA ($M_{w(L\text{-}PS)}=6.1\times10^4$, $M_{w(L\text{-}PMMA)}=6.8\times10^4$); *B1–B4* H-PS and H-PMMA ($M_{w(H\text{-}PS)}=33.6\times10^4$, $M_{w(H\text{-}PMMA)}=33.1\times10^4$)

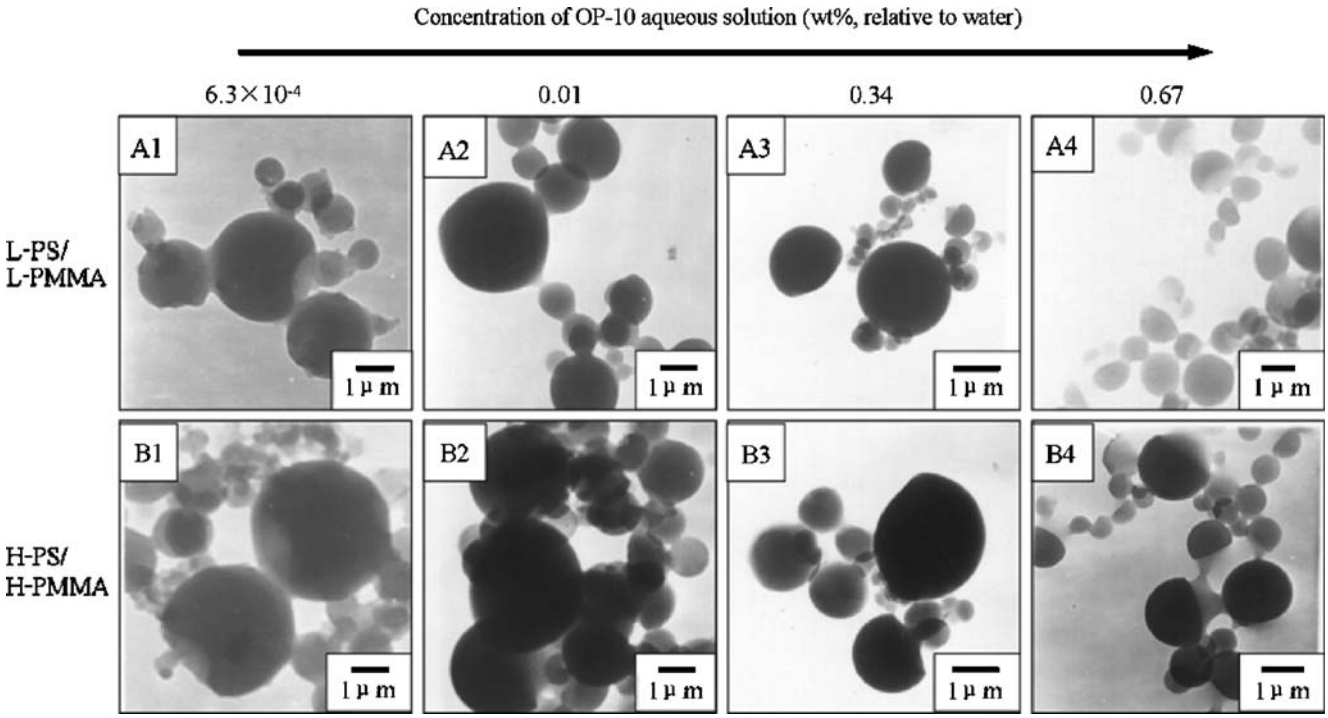

Fig. 2 TEM photographs of PS/PMMA (1/1, *w*/*w*) composite particles prepared by release of toluene from polymer/toluene=1/12 droplets dispersed in various concentration of OP-10 aqueous solutions (weight percent, relative to water): *A1*, *B1* 6.3×10^{-4}; *A2*, *B2* 0.01; *A3*, *B3* 0.34; *A4*, *B4* 0.67. *A1–A4* L-PS and L-PMMA ($M_{w(L\text{-}PS)}=6.1\times10^4$, $M_{w(L\text{-}PMMA)}=6.8\times10^4$); *B1–B4* H-PS and H-PMMA ($M_{w(H\text{-}PS)}=33.6\times10^4$, $M_{w(H\text{-}PMMA)}=33.1\times10^4$)

and 2 B1–B4 have a relative higher molecular weight, which were identified as H-PS and H-PMMA. As shown in Figs. 1 and 2, the morphology of anisotropic PS/PMMA composite particles was influenced both by the concentration of OP-10 aqueous solution and the molecular weight of polymers. For polymers with low molecular weight (L-PS/L-PMMA), the composite particles showed dimple (Figs. 1 A1 and 2 A1), acorn (Figs. 1 A2 and 2 A2) and hemisphere (Figs. 1 A3, A4 and 2 A3, A4) shapes at the OP-10 concentration of 6.3×10^{-4}, 0.01, 0.34, and 0.67 wt.% relative to water, respectively. On the other hand, for polymers with high molecular weight (H-PS/H-PMMA), the composite particles had dimple (Figs. 1 B1 and 2 B1), hemisphere (Figs. 1 B2 and 2 B2) and snowman (Figs. 1 B3, B4 and 2 B3, B4) morphologies at the OP-10 concentration of 6.3×10^{-4}, 0.01, 0.34, and 0.67 wt.% relative to water, respectively. In addition, the dimple and acorn shapes of the PS/PMMA composite particles were caused by the volume contraction of PS phases after hardening of PMMA phase [37]. Moreover, as shown in Fig. 1, the surface of PMMA part was soften and contracted with the increase of phase separation, extremely for the PMMA with lower molecular weight (Fig. 1 A1–A4), since PMMA was weak to electron beams during SEM observation [38]. This phenomenon happened again during TEM observation (Fig. 2) because of the higher electron beams energy. Although the softening and contraction of PMMA parts affected the observation of inner morphology of composite particles, fortunately, this phenomenon can just prove the phase separation of PS and PMMA. The reserved parts (not soften and contracted parts) in Figs. 1 and 2 were PS parts, and the interfaces between PS and PMMA were clear in Figs. 1 and 2. The results could be obtained from Figs. 1 and 2: Phase separation was enhanced with the increase of concentration of OP-10 and molecular weight of polymers. The reason for the formation of anisotropic PS/PMMA composite particles would be discussed in detail through thermodynamic analysis later.

Thermodynamic analysis

It is well known that morphology is controlled by competition between thermodynamic and kinetic factors [44]. The former factor, which drives the system toward a minimum in free energy, determines the equilibrium morphology of the final composite particles, while the latter factor is inclined to thermodynamically favored morphology. When the polymer content (w_P—polymer weight fraction) is higher enough, thermodynamic equilibrium cannot be maintained [37]. As a consequence, the morphology of anisotropic composite particles would remain until the complete removal of the toluene from the

droplets, because the polymer chain mobility would not be high enough for rearrangement. The different shapes of PS/PMMA anisotropic composite particles at different OP-10 concentration and with different molecular weight of polymers can be explained from the viewpoint of total free energy change. The total interfacial free energy change is expressed as [26–30, 45]:

$$\Delta G = \sum \gamma_i A_i - \gamma_0 A_0 \tag{1}$$

where γ_i is the interfacial tension of the ith interface and A_i is the corresponding interfacial area and γ_0 and A_0 are the interfacial tension and interfacial area before phase separation, respectively. In this system, the droplet has three interfaces after phase separation, as shown in Fig. 3b, which corresponded to three interfacial tensions: $\gamma_{PS-T/W}$, $\gamma_{PMMA-T/W}$, and $\gamma_{PS-T/PMMA-T}$. Where $\gamma_{PS-T/W}$, $\gamma_{PMMA-T/W}$, $\gamma_{PS-T/PMMA-T}$ are standing for the interfacial tensions between the PS/toluene phase and water, the PMMA/toluene phase and water, and the toluene phase of PS and PMMA, respectively. For simplicity of thermodynamic analysis, we assume that the final equilibrium state is solely determined by these three interfacial tensions $\gamma_{ij}(i \neq j \neq k = 1, 2, 3)$ [45]. The analysis which yields the same results as that based on minimizing ΔG can be made from a consideration of three spreading coefficients [45]:

$$S_i = \gamma_{jk} - (\gamma_{ij} + \gamma_{ik}). \tag{2}$$

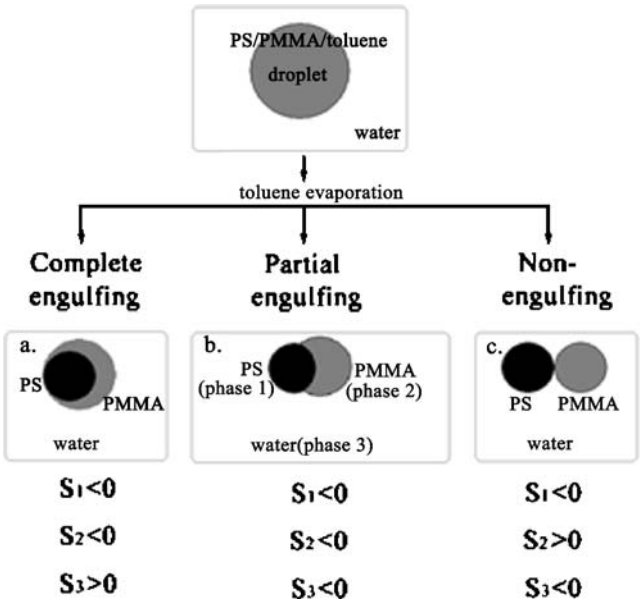

Fig. 3 Schematic models of various shapes corresponding to the three sets of relations for S_i. The *black drop* is phase 1(PS phase), the *gray drop* is phase 3(PMMA phase), and the *medium* is phase 2 (OP-10 aqueous solution)

In current study, we assume $S_1 = S_{PS-toluene}$, $S_2 = S_{water}$, $S_3 = S_{PMMA-toluene}$, the three spreading coefficients would be:

$$S_1 = \gamma_{PMMA-T/W} - \left(\gamma_{PS-T/PMMA-T} + \gamma_{PS-T/W}\right) \tag{3}$$

$$S_2 = \gamma_{PS-T/PMMA-T} - \left(\gamma_{PS-T/W} + \gamma_{PMMA-T/W}\right) \tag{4}$$

$$S_3 = \gamma_{PS-T/W} - \left(\gamma_{PS-T/PMMA-T} + \gamma_{PMMA-T/W}\right). \tag{5}$$

There are three possible sets of S_i values:

$$\text{Complete engulfing} : S_1 < 0,\ S_2 < 0,\ S_3 > 0 \tag{6}$$

$$\text{Partial engulfing} : S_1 < 0,\ S_2 < 0,\ S_3 < 0 \tag{7}$$

$$\text{Nonengulfing} : S_1 < 0,\ S_2 > 0,\ S_3 < 0. \tag{8}$$

These three sets of relations correspond to three different equilibrium morphologies illustrated in Fig. 3a–c. In order to analyzing S_i, each interfacial tension must be known.

For measuring the interfacial tension, it is necessary to consider the partition of OP-10 between toluene phase and water phase firstly, because the partition percentage would affect the interfacial tension. So in the current study, different mass of toluene was added to the aqueous solution of OP-10 at various concentrations to mimic the process of toluene evaporation.

Figures 4 and 5 showed the variations of OP-10 concentrations in aqueous solution and in toluene, respectively, as a weight fraction of toluene relative to the total amount of solution. From Fig. 4, we can see clearly that the OP-10 concentration in the aqueous solution increased with the evaporation of toluene. The lower the toluene concentration relative to total amount, the higher the OP-10 concentration in aqueous solution. As shown in Fig. 5, the OP-10 concentration in toluene phase remained constant (0.01 (Fig. 5a), 0.14 (Fig. 5b), 2.85 (Fig. 5c), and 4.83 wt.% (Fig. 5d) relative to toluene) with the toluene evaporation irrespective of toluene concentration relative to the total amount of solution. Meanwhile, the OP-10 concentration in toluene was much higher than that in aqueous solution. The results above indicate that some fraction of OP-10 would transfer into the polymer/toluene droplets to reach partitioning equilibrium. With the toluene evaporation, excess OP-10 in polymer/toluene droplets would migrate into the aqueous solution, leading to the increase of the OP-10 concentration in the aqueous solution. However, the OP-10

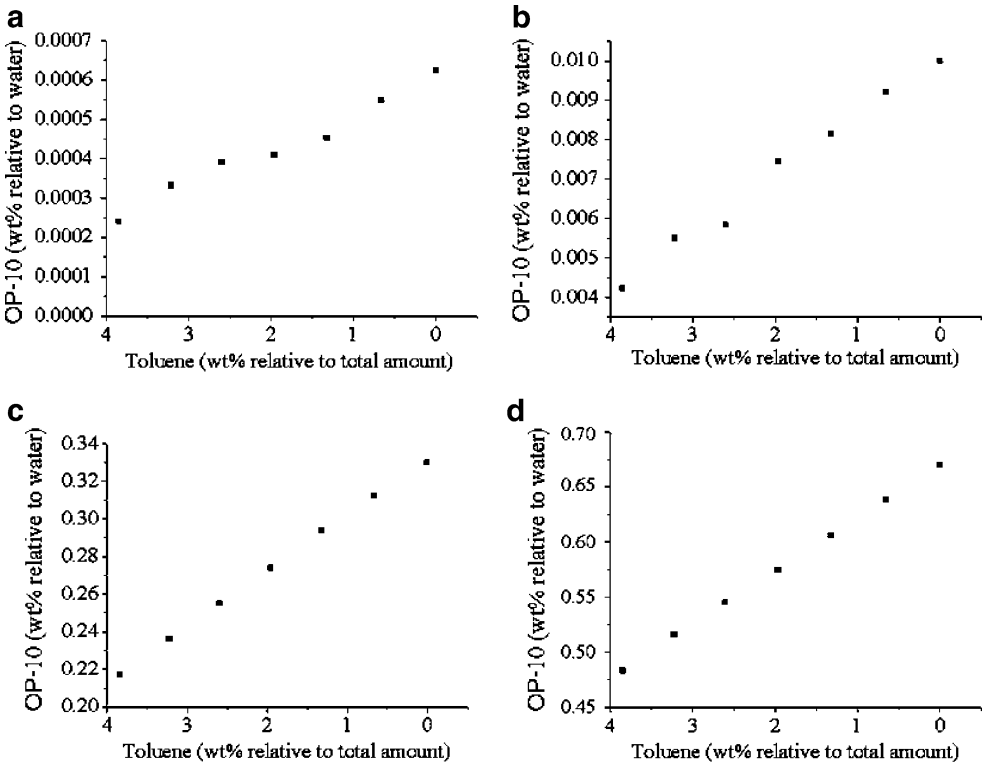

Fig. 4 OP-10 content in the aqueous phases as functions of toluene content (relative to total amount of toluene, water, and OP-10) during evaporation of toluene from dispersions of toluene and various of OP-10 aqueous solution(toluene/water=4/100, *w*/*w*). **a** 6.3×10^{-4}, **b** 0.01, **c** 0.34, and **d** 0.67 (wt.%, relative to water)

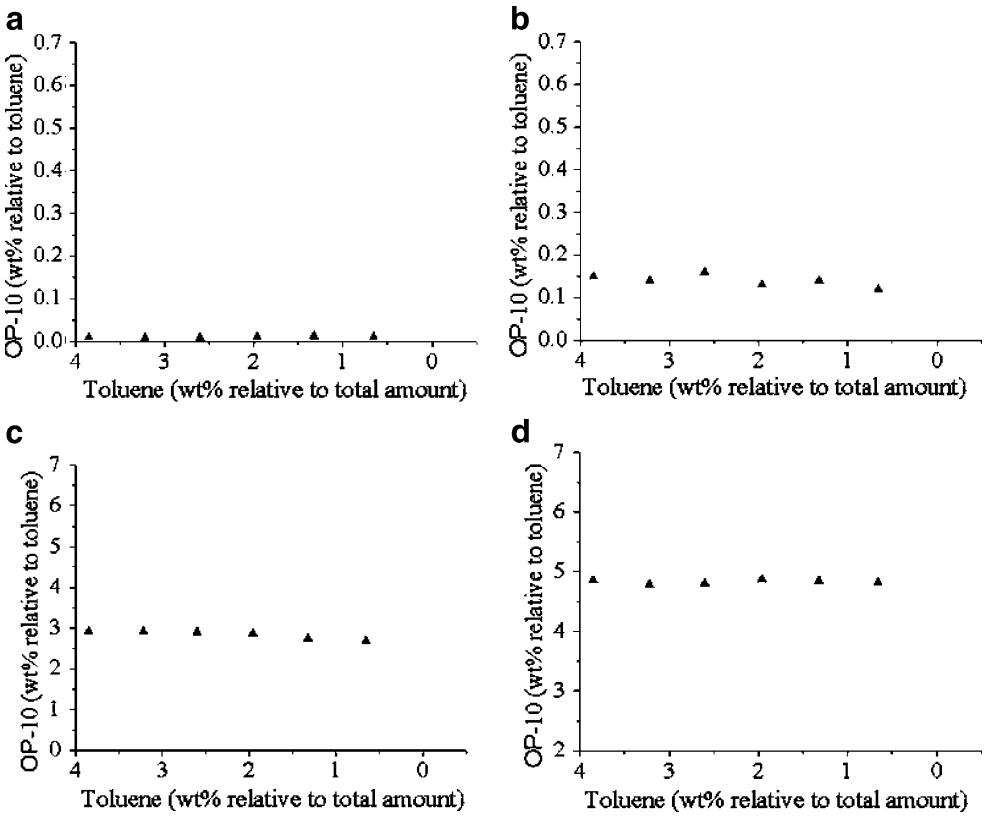

Fig. 5 OP-10 content in the toluene phases as functions of toluene content (relative to total amount of toluene, water, and OP-10) during evaporation of toluene from dispersions of toluene and various of OP-10 aqueous solution(toluene/water=4/100, *w*/*w*). **a** 6.3×10^{-4}, **b** 0.01, **c** 0.34, and **d** 0.67 (wt.%, relative to water)

concentration in the droplets would thus remain constant, which was coincident with the work of Okubo et al. [39].

As the OP-10 concentration in aqueous solution and in toluene can be obtained from isotherm of OP-10 between toluene and water (Figs. 4 and 5), the measurement of interfacial tension between polymer/toluene phase and OP-10 aqueous solution ($\gamma_{P-T/W}$) could be carried out by adding appropriate amount of OP-10 to both phase to simulate the actual experiment conditions during toluene evaporation. Figure 6 shows the interfacial tension between polymer/toluene phase and OP-10 aqueous solutions at various OP-10 concentrations as a function of w_P. As showed in Fig. 6, the $\gamma_{P-T/W}$ remained constant with the increase of w_P from 7.7% to 20% at each OP-10 concentration aqueous solutions. According to other previous reports [29, 46], $\gamma_{P-T/W}$ would be expected to increase with the increasing of w_P; however, the increase of OP-10 concentrations in aqueous solutions during toluene evaporation (Fig. 4) would cause a decrease in $\gamma_{P-T/W}$. That is, the effect of the OP-10 concentration on $\gamma_{P-T/W}$ counteracted the effect of w_P, resulting in the nearly constant of $\gamma_{P-T/W}$ for $7.7\% < w_P < 20\%$. Furthermore, Fig. 6 showed the interfacial tension $\gamma_{P-T/W}$ decreased greatly with the increase of OP-10 concentration from 6.3×10^{-4} to 0.67 wt.% relative to water, for example, $\gamma_{P-T/W}$ with the polymers of L-PS and L-PMMA ($\gamma_{L-P-T/W}$) changed from 13.4 to 1.0 mN/m, while $\gamma_{P-T/W}$ with the polymers of H-PS and H-PMMA ($\gamma_{H-P-T/W}$) changed from 13.1 to 0.8 mN/m. Moreover, the fact that interfacial tension between polymer

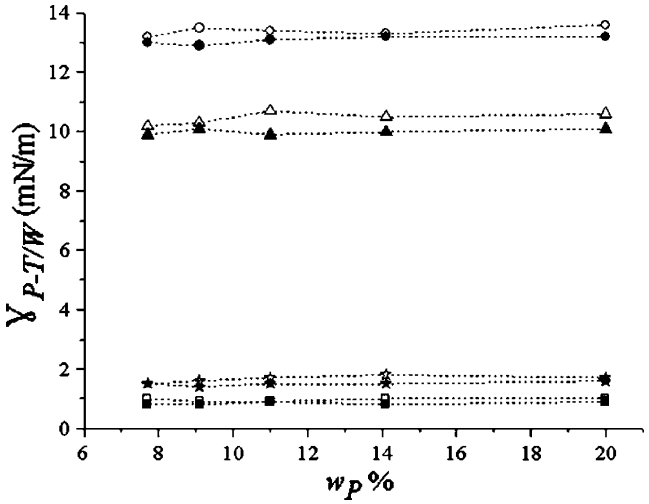

Fig. 6 Interfacial tensions between the polymer phase (PS/PMMA/toluene, 1/1/toluene, *w*/*w*/*w*) and OP-10 aqueous solution as functions of w_P. Concentration of OP-10 aqueous solution (weight percent, relative to water): *open and closed circles* 6.3×10^{-4}, *open and closed triangles* 0.01, *open and closed stars* 0.34, and *open and closed squares* 0.67. Molecular weight of polymers: $M_{w(PS)}=6.1\times10^4$, $M_{w(PMMA)}=6.8\times10^4$ (*open circle*, *open triangle*, *open star*, *open square*); $M_{w(PS)}=33.6\times10^4$, $M_{w(PMMA)}=33.1\times10^4$ (*closed circle*, *closed triangle*, *closed star*, *closed square*)

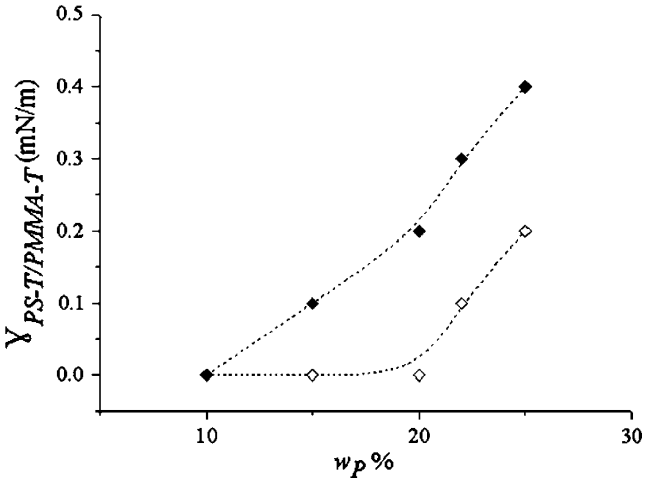

Fig. 7 Interfacial tensions between the PS and PMMA phases as functions of w_P. Polymer solutions were obtained from phase separated PS/PMMA/toluene=1/1/toluene (*w*/*w*/*w*) with different M_w: *closed diamond* $M_{w(PS)}=33.6\times10^4$, $M_{w(PMMA)}=33.1\times10^4$; *open diamond* $M_{w(PS)}=6.1\times10^4$, $M_{w(PMMA)}=6.8\times10^4$

solution and aqueous solution ($\gamma_{P-T/W}$) remained constant at a certain OP-10 concentration aqueous solution indicates that the particles morphology depends on the interfacial tension between PS and PMMA ($\gamma_{PS-T/PMMA-T}$).

The interfacial tension between PS and PMMA phase ($\gamma_{PS-T/PMMA-T}$) was measured without taking account of the partition of OP-10 between the polymer phases, because the nonionic surfactant would not behave as a surface active agent at the interface of PS and PMMA phase [39]. As showed in Fig. 7, the interfacial tension between PS and PMMA phase ($\gamma_{PS-T/PMMA-T}$) increased with the increase of w_P. Furthermore, $\gamma_{H-PS-T/H-PMMA-T}$ was higher than $\gamma_{L-PS-T/L-PMMA-T}$ at a certain w_P.

Comparing Figs. 6 with 7, it could be found that interfacial tension between polymer solution and aqueous solution ($\gamma_{P-T/W}$) was much higher than that between PS and PMMA phase ($\gamma_{PS-T/PMMA-T}$). Assuming that the $\gamma_{PS-T/W}=\gamma_{PMMA-T/W}=\gamma_{P-T/W}$ [39], the spreading coefficients S_i could be calculated according to the Eqs. 3, 4, and 5 as follows:

$$S_1 = -\gamma_{PS-T/PMMA-T} < 0 \tag{9}$$

$$S_2 = \gamma_{PS-T/PMMA-T} - 2\gamma_{P-T/W} \approx -2\gamma_{P-T/W} < 0 \tag{10}$$

$$S_3 = -\gamma_{PS-T/PMMA-T} < 0. \tag{11}$$

Because $S_1<0$, $S_2<0$, and $S_3<0$, according to the Eq. 7 and Fig. 3, the partial engulfing morphology was preferred. It should be noted that the values of $\gamma_{P-T/W}$ decreased with the increase of OP-10 concentration from 6.3×10^{-4} to

0.67 wt.% relative to water, leading to the increase of S_2 ($S_2 \approx -2\gamma_{P-T/W}$). According to Eqs. 6, 7, and 8 and Fig. 3, we can see clearly that the phase separation would be enhanced with the increase of S_2. So the relative low values of $\gamma_{P-T/W}$ at higher OP-10 concentration aqueous solution were very important to the formation of anisotropic particles. That is, with the increase of concentration of OP-10 aqueous solution, phase separation was enhanced, owing to the influence on $\gamma_{P-T/W}$ and S_2. As shown in Fig. 7, the interfacial tension between PS and PMMA with higher molecular weight ($\gamma_{H\text{-}PS-T/H\text{-}PMMA-T}$) was higher than that ($\gamma_{L\text{-}PS-T/L\text{-}PMMA-T}$) with lower molecular weight at a certain w_P. Thus, the values of $S_3 = -\gamma_{PS-T/PMMA-T}$ would decreased with the increase of molecular weight of polymers. As presented in Eqs. 6, 7, and 8 and Fig. 3, the intensity of phase separation would be enhanced with the decrease of S_3. That was to say, phase separation was enhanced with the increase of molecular weight of polymers, owing to the influence on $\gamma_{PS-T/PMMA-T}$ and S_3.

This result consists with the morphology obtained in Figs. 1 and 2. As already discussed, with the toluene evaporation, the interfacial tension between polymer and aqueous phases ($\gamma_{P-T/W}$) decreased with the concentration of OP-10 increasing; moreover, the relative low values of $\gamma_{P-T/W}$ on the basis of the partition of OP-10 to polymer phase were of importance with regard to the formation of anisotropic particles. In addition, the molecular weight was also very important to the final morphology of final particles. The difference of final particles morphology between polymers with lower and higher molecular weight was attributed to the presence of different $\gamma_{PS-T/PMMA-T}$ between PS and PMMA with different molecular weight. This would cause the difference of final anisotropic morphology, such as hemispherical (Fig. 1 A3, A4) with the polymers of L-PS and L-PMMA and snowman-like particles (Fig. 1 B3, B4) with the polymers of H-PS and H-PMMA. In a word, both the concentration of OP-10 aqueous solution and molecular weight of polymers were important for the final morphology of anisotropic composite particles.

Conclusion

Anisotropic PS/PMMA composite particles were prepared by solvent evaporation method. The effects of concentration of OP-10 as a nonionic surfactant and the molecular weight of polymers on the morphology of these anisotropic composite particles were examined. The extent of anisotropic composite particles was enhanced with the increase of the concentration of OP-10 and the molecular weight of polymers. The phase separated PS/PMMA composite particles with polymers of L-PS and L-PMMA ($M_w \approx 6.0 \times 10^4$ g/mol), changed from dimple, via acorn, to hemispherical structures with increasing OP-10 concentration. Otherwise, the morphology of PS/PMMA composite particles with polymers of H-PS and H-PMMA ($M_w \approx 3.3 \times 10^5$ g/mol), changed from dimple, via hemispherical, to snowman-like shapes.

The complicated phase separation during the preparation of anisotropic particles can be well predicted by the spreading coefficients analysis. These findings provide a better theoretic morphological prediction and a practically preparation method of anisotropic composite particles. Further extensive work is underway in our lab.

Acknowledgment The authors gratefully acknowledge the National Natural Science Foundation of China (nos. 50573070 and 50773073) and Program for Changjiang Scholars and Innovative Research Team in University for the support of this work.

References

1. Mischenko MI, Hovenier JW, Travis LD (2000) Light scattering by nonspherical particles: theory, measurements, applications. Academic, San Diego
2. Larson RG (1998) The structure and rheology of complex fluids. Oxford University Press, New York
3. Jogun SM, Zukoski CF (1999) J Rheol 43:847
4. Glotzer SC (2004) Science 306:419
5. Zhang ZL, Horsch MA, Lamm MH, Glotzer SC (2003) Nano Lett 3:1341
6. Glotzer SC, Horsch MA, Iacovella CR, Zhang ZL, Chan ER, Zhang X (2005) Curr Opin Colloid Interface Sci 10:287
7. Binks BP, Fletcher PDI (2001) Langmuir 17:4708
8. Murphy CJ (2002) Science 298:2139
9. Pickering SU (1907) J Chem Soc 91:2001
10. Dinsmore AD, Hsu MF, Nikolaides MG, Marquez M, Bausch AR, Weitz DA (2002) Science 298:1006
11. Bink BP, Clint JH (2002) Langmuir 18:1270
12. Jana NR, Gearheart L, Murphy CJ (2001) J Phys Chem B 105:4065
13. Jin R, Cao YW, Mirkin CA, Kelly KL, Schatz GC, Zheng JG (2001) Science 294:1901
14. Okubo M, Katsuta Y, Matsumoto T (1980) J Polym Sci Poly Lett Ed 18:481
15. Okubo M, Yamada A, Matsumoto T (1980) J Polym Sci Polym Chem Ed 16:3219
16. Okubo M, Ando M, Yamada A, Katsuta Y, Matsumoto T (1981) J Polym Sci Polym Lett Ed 19:143
17. Morgan LW (1982) J Appl Polym Sci 27:2033
18. Okubo M, Katsuta Y, Matsumoto T (1982) J Polym Sci Polym Lett Ed 20:45
19. Lee DI, Ishikawa T (1983) J Polym Sci Polym Chem Ed 21:147
20. Min TI, Klein A, El-aasser MS, Vanderhoff JW (1983) J Polym Sci Polym Lett Ed 21:2845
21. Dimonie V, El-aasser MS, Klein A, Vanderhoff JW (1984) J Polym Sci Polym Chem Ed 22:2197
22. Muroi S, Hashimoto H, Hosoi K (1984) J Polym Sci Polym Chem Ed 22:1365
23. Cho I, Lee KW (1985) J Appl Polym Sci 30:1903
24. Merkel MP, Dimonie VL, El-aasser MS, Vanderhoff JW (1987) J Polym Sci A Polym Chem 25:1755

25. Okubo M, Ikegami K, Yamamoto Y (1989) Colloid Polym Sci 267:193
26. Lee S, Rudin A (1989) Makromol Chem Rapid Commun 10:655
27. Sheu HR, El-aasser MS, Vanderhoff JW (1990) J Polym Sci A Polym Chem 28:629
28. Sheu HR, El-aasser MS, Vanderhoff JW (1990) J Polym Sci A Polym Chem 28:653
29. Okubo M (1990) Makromol Chem Macromol Symp 35/36:307
30. Shen S, El-aasser MS, Dimonie VL, Vanderhoff JW, Sudol ED (1991) J Polym Sci A Polym Chem 29:857
31. Lee S, Rudin A (1992) J Polym Sci A Polym Chem 30:2211
32. Jonsson JE, Hassander H, Tornell B (1994) Macromolecules 27:1932
33. Dimonie VL, Daniels ES, Shaffer OL, El-Aasser MS (1997) Emulsion polymerization and emulsion polymers. In: Lovell PA, El-Aasser MS (eds) Wiley, New York, Chapter 9, pp 293–326
34. Rajatapiti P, Dimonie VL, El-aasser MS, Vratsanos MS (1997) J Appl Polym Sci 63:205
35. Karlsson O, Hassander H, Wesslen B (1997) J Appl Polym Sci 63:1543
36. Okubo M, Saito N, Fujibayashi T (2005) Colloid Polym Sci 283:691
37. Okubo M, Saito N, Kagari Y (2006) Langmuir 22:9397
38. Ahmad H, Saito N, Kagawa Y, Okubo M (2007) Langmuir 24:688
39. Saito N, Nakatsuru R, Kagari Y, Okubo M (2007) Langmuir 23:11506
40. Tanaka T, Nakatsuru R, Kagari Y, Saito N, Okubo M (2008) Langmuir 24:12267
41. Karlsson OJ, Hassander H, Wesslen B (2000) J Appl Polym Sci 77:297
42. Stubbs JM, Sundberg DC (2006) J Appl Polym Sci 102:945
43. Chen YC, Dimonie V, El-Aasser MS (1992) J Appl Polym Sci 46:691
44. Sundberg DC, Durant YG (2003) Polym React Eng 11:379
45. Torza S, Mason SG (1970) J Colloid Interface Sci 33:67
46. Siow KS, Patterson D (1973) J Phys Chem 77:356